48th AIAA/ASME/SAE/ASEE Joint Propulsion Conference & Exhibit
30 July - 01 August 2012, Atlanta, Georgia

AIAA 2012-3930

VASIMR® VX-200 Improved Throttling Range

Benjamin W. Longmier[1], Jared P. Squire[2], Chris S. Olsen[3], Leonard D. Cassady[4], Maxwell G. Ballenger[5], Mark D. Carter[6], Andrew V. Ilin[7], Tim W. Glover [8], Greg E. McCaskill[9], Franklin R. Chang Díaz[10],
Ad Astra Rocket Company, Webster, TX 77598, USA

Edgar A. Bering, III[11]
University of Houston, Departments of Physics and ECE, Houston, TX 77204, USA

Testing of the VX-200 engine was performed over a wide throttle range in a vacuum facility with sufficient volume and pumping to permit exhaust plume measurements at low background pressures and sufficiently large charge exchange mean free paths. Experimental results are presented with the VX-200 engine installed in a 150 m^3 vacuum chamber with an operating pressure below $1x10^{-3}$ Pa ($1x10^{-5}$ Torr), and with an exhaust plume diagnostic measurement range of 5 m in the axial direction and 1 m in the radial directions. Measurements of plasma flux, RF power, and neutral gas flow rate, combined with knowledge of the kinetic energy of the ions leaving the VX-200 engine, are used to determine the ionization cost of argon and krypton in the first stage helicon plasma discharges. Experimental data on ionization cost, ion fraction, exhaust plume expansion angle, thruster efficiency, and total force are presented that characterize the VX-200 engine performance over a wide throttling range from 15 kW to 200 kW total RF power. A semi-empirical model of the thruster efficiency as a function of specific impulse was developed to fit the experimental data, and reveals a second stage Ion Cyclotron Heating (ICH) RF power coupling efficiency of 85%. Operation at an RF power level of 200 kW yields a thruster efficiency of 72%±9% at a specific impulse of 4900±300 s. A high thrust-to-power operating mode was characterized over a wide parameter space with a maximum thrust to power ratio of 51 mN/kW at a specific impulse of 1660 s for a ratio of ICH RF power to helicon RF power of 0.7:1.

[1] Principal Research Scientist, Ad Astra Rocket Company, ben.longmier@adastrarocket.com
[2] Director of Research, Ad Astra Rocket Company, jared.squire@adastrarocket.com
[3] Research Scientist, Ad Astra Rocket Company, chris.olsen@adastrarocket.com
[4] Lead Engineer, Ad Astra Rocket Company, lcassady@adastrarocket.com
[5] Staff Scientist, Ad Astra Rocket Company, maxwell.ballenger@adastrarocket.com
[6] Director of Technology, Ad Astra Rocket Company, mark.carter@adastrarocket.com
[7] Computational Research Lead, Ad Astra Rocket Company, andrew.ilin@adastrarocket.com
[8] Director of Development, Ad Astra Rocket Company, tim.glover@adastrarocket.com
[9] Senior RF Engineer, Ad Astra Rocket Company, greg.mccaskill@adastrarocket.com
[10] Chief Executive Officer, Ad Astra Rocket Company, aarcinfo@adastrarocket.com
[11] Professor, Physics and ECE, University of Houston, eabering@uh.edu

Nomenclature

DC	= direct current
e	= electron charge [C]
$E_{\|\|}, E_{\perp}$	= ion kinetic energy [eV]
E_i	= ionization cost [eV]
E_1	= ion kinetic energy after helicon [eV]
F	= jet force (thrust) [N]
g	= gravitational acceleration [m/s^2]
GEO	= geostationary Earth orbit
HTSC	= high temperature superconductor
ICH	= ion cyclotron heating
I_{ion}	= ion current in the exhaust [A]
I_{sp}	= specific impulse [s]
LEO	= low Earth orbit
LTSC	= low temperature superconductor
$\dot{m}$	= propellant flow rate [kg/s]
m_i	= ion mass [kg]
P_{jet}	= jet power [W]
$P_{1,RF}$	= helicon RF power [W]
$P_{2,RF}$	= ICH RF power [W]
PMFS	= plasma momentum flux sensor
RF	= radio frequency
RPA	= retarding potential analyzer
VASIMR	= Variable Specific Impulse Magnetoplasma Rocket
z, r	= cylindrical coordinates [m]
β	= plasma beta (kinetic to magnetic pressure ratio)
η_B	= booster (ICH) efficiency
η_n	= nozzle efficiency
η_T	= thruster efficiency, jet power/RF power
θ	= exhaust divergence half-angle [deg]

I. Introduction

High-power electric propulsion thrusters can reduce propellant mass for heavy-payload orbit-raising missions and cargo missions to the Moon and near Earth asteroids and can reduce the trip time of robotic and piloted planetary missions.[1-4] The Variable Specific Impulse Magnetoplasma Rocket (VASIMR®) VX-200 engine is an electric propulsion system capable of processing power densities on the order of 6 MW/m^2 with a high specific impulse (2000 s to 5000 s) and an inherent capability to vary the thrust and specific impulse at a constant input power. The potential for long lifetime is due primarily to the radial magnetic confinement of both ions and electrons in a quasi-neutral flowing plasma stream, which acts to significantly reduce the plasma impingement on the walls of the rocket core. High temperature ceramic plasma-facing surfaces handle the thermal radiation, the principal heat transfer mechanism from the discharge. The rocket uses a helicon plasma source[5,6] for efficient plasma production in the first stage. This plasma is energized further by an ion cyclotron heating (ICH) RF stage that uses left hand polarized slow mode waves launched from the high field side of the ion cyclotron resonance. Useful thrust is produced as the plasma accelerates in an expanding magnetic field, a process described by conservation of the first adiabatic invariant as the magnetic field strength decreases in the exhaust region of the VASIMR.[7-9]

II. Experimental Setup and Method

A. VX-200 Engine

The VX-200 engine is an experimental VASIMR prototype designed to operate at 200 kW of input DC electrical power. The device provides an end-to-end integrated test of the primary VASIMR components in a vacuum environment with the goal of measuring and improving the system performance. A majority of the VX-200 engine components are located within the vacuum chamber, with only the solid-state RF generators, superconducting magnet power supplies, and cryocoolers kept at atmospheric pressure.

The superconducting magnet, support structure, rocket core, engine sensors, and electrical components are operated within the vacuum chamber. Figure 1 shows a schematic of the VX-200 engine installed inside the vacuum chamber and the approximate shape of the magnetic field flux lines within the core and magnetic nozzle.

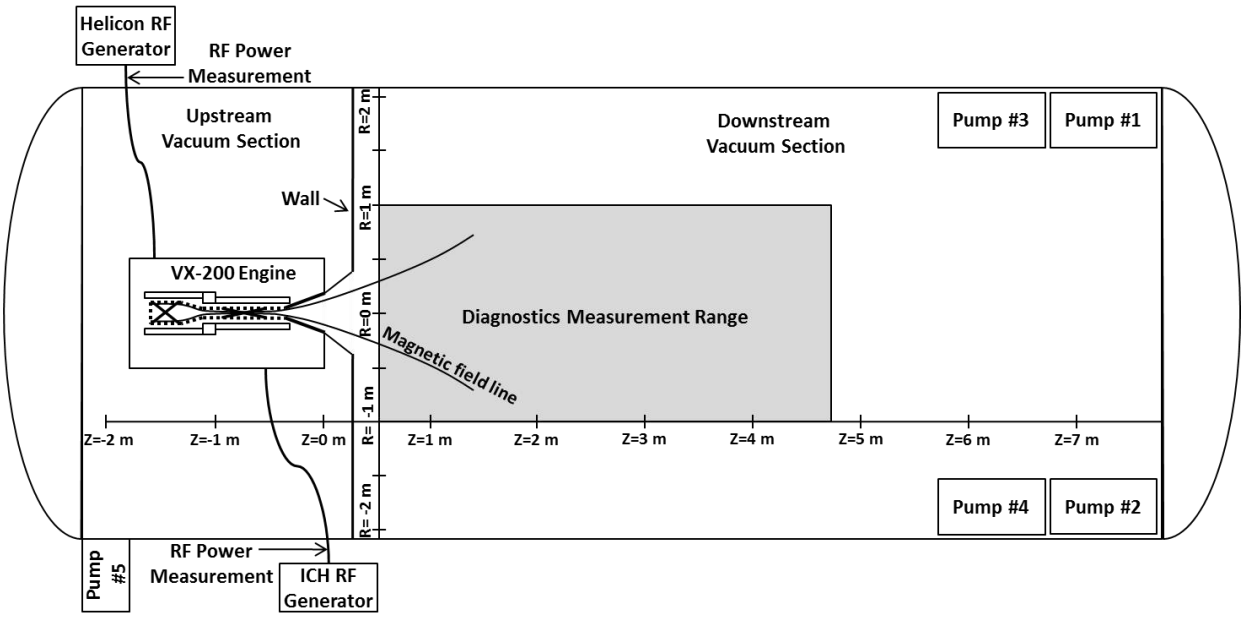

Figure 1. Schematic of the 10 m long x 4.2 m diameter vacuum chamber and the VX-200 engine, RF generators, RF power measurement location, vacuum partitioning wall, representative magnetic field lines, and the measurement range of the exhaust plume diagnostics.

The core of the VX-200 engine is defined as the components that physically surround the plasma and intercept the bulk of the waste heat radiated by the plasma column. The VX-200 engine is restricted to pulses of less than one minute owing to temperature limitations of certain seals and joints in the rocket core. The helicon stage launches a right-handed circularly polarized wave, that produces a cold plasma. A pressure gradient drives the plasma flow through a magnetic choke into the ion cyclotron heating (ICH) stage where another RF coupler launches a wave that preferentially heats the ions in a single pass.[9]

The VX-200 engine RF generators convert facility DC power to RF power and perform impedance matching between the RF generator output and the rocket core, Fig. 2. The RF generators were custom built by Nautel Ltd., model numbers VX200-1 (helicon generator), and VX200-2 (ICH generator). The VX200-1 RF generator is rated up to 48±1 kW RF with a 91±1% efficiency and a specific mass of 0.85±0.02 kg/kW. The VX200-2 generator is rated up to 172±1 kW RF with a 98±1% efficiency and a specific mass of 0.506±0.003 kg/kW. The generator efficiencies were determined by independent testing performed by Nautel Ltd., which included a direct measurement of input power and calorimetry of the dissipated power in the generator.

The exhaust velocity of the ions increases as the coupled ICH power increases. Coupled RF power is defined as the RF power that is injected by the helicon and/or ICH couplers and is inductively absorbed by the plasma column or radiatively lost by the RF couplers. The coupled RF power is determined by subtracting the

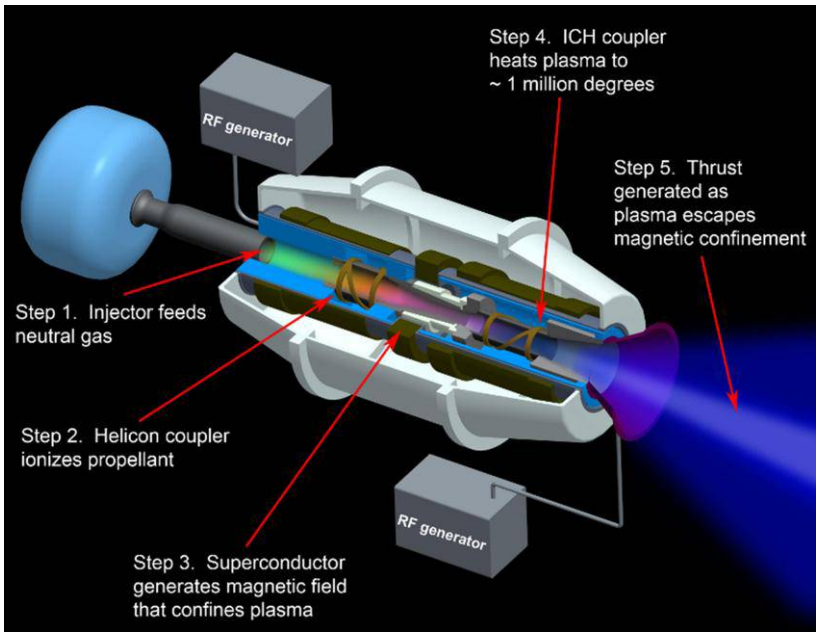

Figure 2. Schematic of the VASIMR VX-200 engine.

power losses in the RF matching network and RF transmission line from the measured RF power at the RF generator output, Fig. 1. Losses in the matching networks and transmissions lines are calculated based on network analyzer measurements of circuit impedance. The efficiency was determined to be 96% for both the helicon and ICH RF circuits.

The VX-200 engine low temperature superconducting (LTSC) magnet is cooled to 6 K by a pair of Sumitomo cryocooler (RDK-408D2) / cryocompressor (CSW-71) units with a maximum combined power draw of 15 kW. The VX-200 engine LTSC magnet produces a maximum magnetic field strength of 2 tesla that results in highly confined electrons and argon ions within the engine core. Estimates for cryocooler power draw for flight designs are less than 3 kW total for high temperature superconducting (HTSC) magnets cooled to 50 K. The magnetic field in the VX-200 engine is responsible for efficient ion cyclotron coupling of the RF energy to the ions within the quasi-neutral flowing plasma. The applied expanding magnetic field converts perpendicular ion kinetic energy, $E_{\perp}$, to directed parallel ion kinetic energy, $E_{\parallel}$, through conservation of the magnetic moment and conservation of the ion's total kinetic energy.[7-9] The location at which 90% of the perpendicular ion energy is converted into parallel ion energy, $E_{\parallel}/(E_{\parallel} + E_{\perp}) = 0.9$, occurs at z = 0.05 m, r = 0 m.

An ambipolar ion acceleration has also been observed[10] and is believed to be the result of the plasma interaction with the magnetic field gradient in the expanding magnetic nozzle of the VX-200 engine, similar to the Boltzmann relation but with a varying electron temperature. The ambipolar ion acceleration typically results in an additional directed ion velocity of 5 to 10 km/s, where the energy for this process comes from the electron energy distribution function as a result of electron and ion interaction with a weak electric field in the magnetic nozzle, which ranges in strength from 10 to 20 V/m depending on system parameters.

The data presented in this paper was taken during quasi steady-state operation, up to 30 s in duration. The neutral pressure gradients within the VX-200 engine and the vacuum system equalize within 0.8 s of the initial startup. From 0.8 s through 30 s, the neutral pressure throughout the VX-200 engine and vacuum system are steady-state values. Data for the thruster efficiency calculations was taken during the steady-state portion of the VX-200 operation. The propellant mass flow rate was varied between 50 to 160 mg/s for argon and 100 to 250 mg/s for krypton and was measured by use of a calibrated proportional flow control valve flow controller in addition to a calibrated (NIST traceable) thermal-based mass flow meter that was in-line at the high pressure end of the propellant feed system.

B. Vacuum Facility

The VX-200 engine is installed, as shown in Figure 1, inside a stainless steel vacuum chamber[11,12] that is 4.2 m in diameter and 10 m long with a volume of 150 m^3 including the end caps. One end opens fully for access to the entire inner diameter of the chamber. The vacuum chamber is partitioned into two sections: an upstream section and a downstream section. The upstream vacuum section (where the VX-200 engine is located) is kept at a pressure one to two orders of magnitude lower than the downstream, or exhaust, vacuum section, while the VX-200 is firing. The partition, located at z = 0.2 m, helps to prevent arcing and glow discharges near the high voltage transmission lines and matching circuit components. Similar work related to the challenges of operating a RF antenna in vacuum was performed by West et al.[13] The facility used three CVI Torr Master internal cryopumps in the downstream section of the vacuum chamber and provided an Ar pumping speed of ~160,000 l/s. The exhaust section pressure was less than $1x10^{-3}$ Pa ($1x10^{-5}$ Torr) for the first 0.8 s, and less than $1x10^{-2}$ Pa ($1x10^{-4}$ Torr) from 0.8 s to 30 s of operation, yielding a charge exchange mean free path of ~10 m and ~1 m respectively. The base pressure of the vacuum chamber was less than $7x10^{-6}$ Pa ($5x10^{-8}$ Torr) before each firing.

C. Flux Probe Array

The ion flux was measured with an array of ten 0.64 cm diameter molybdenum planar probes of a top hat design[14] that were biased into the ion saturation regime, -15 V with respect to chamber ground. Full I-V traces were taken with a Langmuir probe with a guard ring of the same dimensions and analyzed to ensure that the ion flux probes were biased $3T_e$ more negative than the floating potential. Ion flux measurements were taken both during quick startup shots, where the ambient neutral gas pressure was below $1x10^{-3}$ Pa ($1x10^{-5}$ Torr), and during translating radial profiles where the sustained neutral argon pressure within the vacuum chamber was $1x10^{-2}$ Pa ($1x10^{-4}$ Torr).

D. Plasma Momentum Flux Sensor

A plasma momentum flux sensor (PMFS), described in detail elsewhere,[15] was used to measure the force of the plasma ejected from the VX-200 engine. The PMFS consists of a 9 centimeter diameter electrically floating graphite target disc attached to a stiff 10 centimeter long insulating alumina rod. The stiff alumina rod connected to a small

titanium bar, 5.72 cm by 1.30 cm, where a series of 4 high output semiconductor strain gauges measure the strain caused by the torque from the applied plasma impact force. The PMFS was calibrated with the method employed by Chavers et al.[16,17] A small graphite shield was used to shield the entire titanium bar and strain gauge assembly from the flowing plasma stream.

The resolution of the PMFS was 0.1 mN, which allowed for sufficiently sensitive measurements of the force applied by the exhaust plasma. The natural frequency of oscillations was 40 Hz, and this oscillation was filtered out during the analysis of radial or temporal force profiles, though the temporal data is limited in resolution to ~1/40 s. The use of the PMFS technique was previously compared and validated with a more traditional inverted pendulum thrust stand in a 9 m long, 6 m diameter vacuum chamber using the P5 Hall thruster.[15] Other groups have employed similar plasma momentum flux sensors, the use of which has been promising, due to size, cost, and configuration limitations commonly associated with thrust stands.[18-27]

E. Retarding Potential Analyzer

Measurements of the ion energy in the exhaust region were made with a 4 grid retarding potential analyzer (RPA)[9] of a new design that was optimized for operation in a plasma environment with plasma densities up to 10^{20} m^{-3} and a heat flux of up to 10 MW/m^2. The attenuator and repulsion grids were 635-wire/cm and 100-wire/cm stainless steel mesh respectively, spaced 3 mm apart with alumina spacers. The opening apertures to the RPA consisted of 21 0.2 mm holes space evenly over a 1 cm diameter area of pyrolytic graphite which yielded a 1% transparency. The 21 entrance holes' length to diameter ratio was such that they exhibited an 11-degree pitch angle acceptance. A four-grid configuration was used, with entrance attenuator, electron suppressor, ion analyzer, and secondary suppressor grids. The ion exhaust velocity is deduced from the raw data by means of least-squares fits of drifting Maxwellians to the current-voltage data from the RPA.[28-31] RPAs work by varying a repelling potential on the ion analyzer grid. Ions with a flow kinetic energy greater than the retarding electrostatic potential energy reach the collector. Since multiply ionized ions do not have the same ion cyclotron frequency, they will have a very different energy distribution and flow velocity than the singly ionized ions that are accelerated by the ICH stage of the VX-200 engine. Multiple component ion populations appear in RPA data as a stepped current-voltage characteristic, which must be analyzed by fitting a multi-component distribution. Previous studies of a 10% deuterium 90% hydrogen plasma in a VASIMR device have demonstrated that a plasma with a 10% component with a factor of 2 different m/q ratio can easily be resolved.[32] Based on these prior results, it is a conservative estimate that the RPA would have seen a resolvable 2nd lower energy Maxwellian population with a detection level of 5% of the singly ionized Maxwellian population.[32]

F. Optical Spectrometer

Data from an Ocean Optics USB4000 fiber optic spectrometer was used to look for spectral emission lines from neutral argon (ArI), singly ionized argon (ArII) doubly ionized argon (ArIII), triply ionized argon (ArIV), and trace impurities in the plume at z = 0.05 m, r=0 m. The spectrometer had a range of 200 nm to 1100 nm with a resolution of 0.3 nm. The spectrometer used a 2 degree collimation lens and looked through the diameter of the exhaust plume at a matte black plate on the far side of the plume, which was used to absorb reflected light from stray sources. The National Institute of Standards and Technology (NIST) atomic spectra database was used to identify ArI, ArII, ArIII, ArIV and other spectral lines.[33]

III. Experimental Results and Discussion

For the first time, the total force from the VASIMR VX-200 engine has been measured at the full operating RF power level of 200 kW. Using the PMFS the force density within the exhaust plume of the VX-200 engine was measured as a function of the radial and axial position. To determine the total force produced by the VX-200 engine, the force density over one full radius of the exhaust plume, as shown in Fig. 3a, was integrated using azimuthal symmetry. As the coupled RF power was increased from 28 kW to 200 kW, the total force produced by the VX-200 engine was measured using the PMFS. As shown in Figure 3b, the total force increased with increasing ICH coupled RF power as expected.

For the data presented in Fig 3a and Fig 3b the PMFS was located at z = 0.4 m, where $E_{\parallel}/(E_{\parallel} + E_{\perp}) = 0.98$. The PMFS was 0.09 m in diameter; small compared to the total exhaust plume diameter of approximately 0.7 m. The representative set of force density data for Figure 3a were taken at 14 samples/cm radially from r = 0 m to r = 0.4 m, and 1 sample every 0.1 m axially from z = 0.4 m to z = 2.6 m. The VX-200 engine was operated with 107 mg/s of Ar propellant, a peak magnetic field strength of 2 tesla, a helicon coupled RF power level of 28 kW and an

ICH coupled RF power level of 90 kW for the data presented in Figure 3a, and an ICH power level range of 0 kW to 172 kW for the data presented in Figure 3b. The total computed force had less than a 1% error from measurements made at various axial locations from z = 0.4 m to 2.6 m.

A. Optimized Thruster Performance

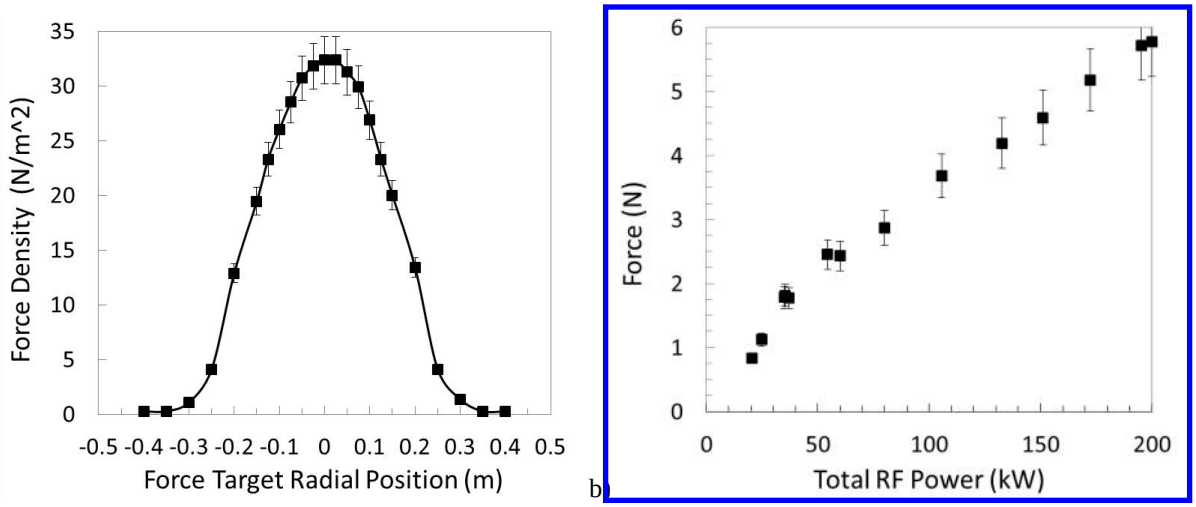

a) b)

Figure 3. A measured diameter profile of the VX-200 engine force density during a 108 kW firing, a), and the total force of the VX-200 engine as a function of the RF power coupled to the argon plasma, b).

Nozzle Divergence Angle

The ion current density and force density were mapped over a large region of the exhaust plume, z=0.4 m to 2.6 m axially with a resolution of 0.1 m, and r=0 m to ±0.75 m radially with a resolution of 0.7 mm, with the flat faces of the ion current density probes and the PMFS always in a plane orthogonal to the VX-200 engine axis, i.e. always facing in the direction parallel to the engine axis. This mapping was performed at a total coupled RF power level of 118 kW and a neutral background pressure of $1x10^{-3}$ Pa ($1x10^{-5}$ Torr). The plasma jet data exhibited a well-defined edge in both ion current density and force density,[11] similar to other helicon based devices.[34] Assuming azimuthal symmetry, the conical boundary contour that surrounded 90% of the integrated ion current density and force density was calculated. The angle of that boundary line relative to the VX-200 engine axis, θ, provided an estimate of the exhaust divergence half-angle. The ion current density data yielded a divergence half-angle of 20±2 degrees, while the force density data yielded a divergence half-angle of 18±2 degrees. The half angles were found by radially integrating the ion current density and force density to 90% of the total ion current and total force. The ion flux probe and the PMFS were not rotated such that the ions impacted normal to these surfaces, but were left facing in the direction parallel to the VX-200 engine centerline and translated radially. The conical nozzle correction factor[35] can be used to estimate the fraction of directed momentum to total flow momentum. Here, this correction factor is defined as the nozzle efficiency when expressed as a percentage,

$$\eta_n = \frac{1}{2}(1 + \cos\theta). \qquad \text{Eqn. 1}$$

The integrated current density and force density data yield a nozzle efficiency of 97% and 98% respectively for the plume in the region from z = 0.4 m to z = 1.6 m. Plume divergence angle and plasma detachment details farther downstream than z = 1.6 m are as of yet unknown. For the following system efficiency analysis, the more conservative 97% nozzle efficiency was used. This estimate was consistent with particle trajectory modeling[36] that predicted a nozzle efficiency of 90%. Calculations based on a MHD theory[37] that factors in possible drag effects due to the plasma leaving the high magnetic strength zone yield a nozzle efficiency of 87%, though recent experimental data show that the plasma detachment from the magnetic nozzle does not follow MHD predictions.[38] Recent data with argon plasma suggest the ions separate at higher magnetic field strengths than traditional MHD fluid models of super-alfvenic flow predict. The electrons remain magnetized in the magnetic nozzle region and separate farther

downstream near the β = 1 transition. Research on the detachment mechanisms within the magnetic nozzle continue to be an active area of research.[39]

The total thruster efficiency, η_T, of the VX-200 engine was determined by dividing the total RF power coupled to the plasma by the thruster jet power, where the jet power is defined as

$$P_{jet} = \frac{F^2}{2\dot{m}} \quad , \qquad \text{Eqn. 2}$$

where F is the total force produced by the rocket and $\dot{m}$ is the total mass flow rate of propellant. Dividing equation 2, by the total RF power coupled to the plasma yields

$$\eta_T = \frac{P_{jet}}{P_{1,RF}+P_{2,RF}} \quad , \qquad \text{Eqn. 3}$$

where $P_{1,RF}$ and $P_{2,RF}$ represent the RF power coupled to the helicon and ICH stages of VX-200 engine respectively. Specific impulse is defined as

$$I_{SP} = \frac{F}{\dot{m}g} \qquad \text{Eqn. 4}$$

Optimized Thrust-to-Power

Many electric propulsion spacecraft and satellite operations can benefit economically if the transfer times are reduced. Additionally, many military operational satellites can benefit from faster orbital transfer times. Optimizing the Thrust-to-Power (T/P) ratio, that is, the ratio of input RF power to the amount of thrust that is generated, can lead to significant savings in orbital transfer times given a fixed power system such as solar panels with a finite collection area. The T/P ratio of the VX-200 prototype was optimized over a wide range of specific impulse values from 780 s to 4900 s, with a peak T/P of 51 mN/kW at a specific impulse of 1660 s, and an ICH to helicon power ratio of 0.7:1, Fig. 4. These optimum T/P values were found at each specific impulse setting by fixing the ratio of the input ICH power to input helicon power and then finding a propellant flow rate that maximized the T/P. Each data point on Fig. 4 represents hundreds of firings taken during the experimental campaign in an effort to find the optimum T/P ratio. The average difference in performance between two different shots with the same settings was less than 1%. This procedure was repeated for a variety of ICH to Helicon power levels and for a variety of total power levels. Figure 4 represents the optimized values of T/P for a variety of mass flow settings and ICH to helicon power levels and total power levels. However, the higher power levels generally resulted in higher T/P values since the VX-200 prototype was designed for highest efficiency at a total power level of 200 kW.

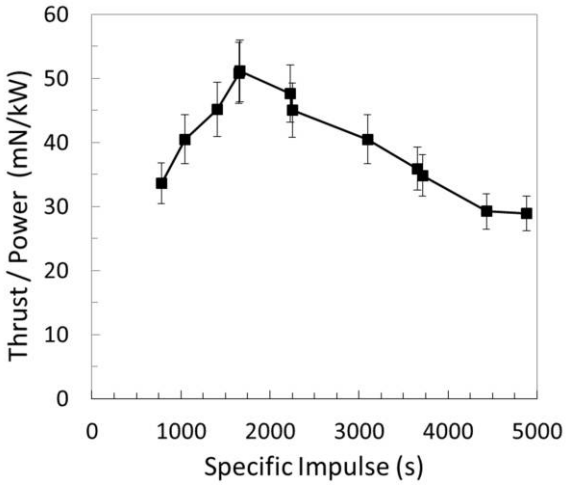

Figure 4. Thrust to RF power ratio as a function of the specific impulse for argon propellant. A maximum in thrust to power occurs for a specific impulse value of 1660 s.

The data in Fig. 4 represents the optimized T/P values for the VX-200 prototype in its present configuration with a fourth generation ICH coupler design. The data was taken for argon propellant only, and section C points to a semi-empirical model that was fit to the argon data and then extrapolated for krypton operation. As a point of reference to the data presented in Fig. 4, the highest power Hall Effect Thruster that has been operated in spaceflight has a throttle table that includes T/P ratios from 40 to 60 mN/kW over a specific impulse range from 1000 s to 2600s.[40]

Optimized Thruster Efficiency

Figure 5 shows the total thruster efficiency as a function of the ratio of P_{ich}/P_{hel}, a), and the specific impulse, b), where the specific impulse was calculated using Eqn. 4 with measured values of force and propellant flow rate, and the total thruster efficiency was calculated using Eqn. 3. For data presented in Fig. 5, the VX-200 engine used a propellant flow rate from 80 to 110 mg/s, a helicon coupled RF power level from 15 to 30 kW, and an ICH coupled RF power level from 0 to 172 kW, which yielded results that show a total force of up to 5.8±0.4 N, at an I_{sp} of 4900±300 s, and a 72±9% thruster efficiency. Previous RPA data was used to corroborate the PMFS measurements. RPA measurements were taken at power levels up to 136 kW and matched the PMFS measurements with an error of less than 3%. At RF power levels up to 136 kW, the RPA was used to verify the PMFS results and reported a mean ion flow velocity of 32.8 km/s with an ion temperature of ~50 eV in the frame of reference moving with the beam. RPA measurements were not possible at power levels higher than 136 kW as the power density of the plasma exhaust led to RPA grid degradation. However, RPA measurements showed at most a 3% error compared to the PMFS at a total RF power level of 136 kW.

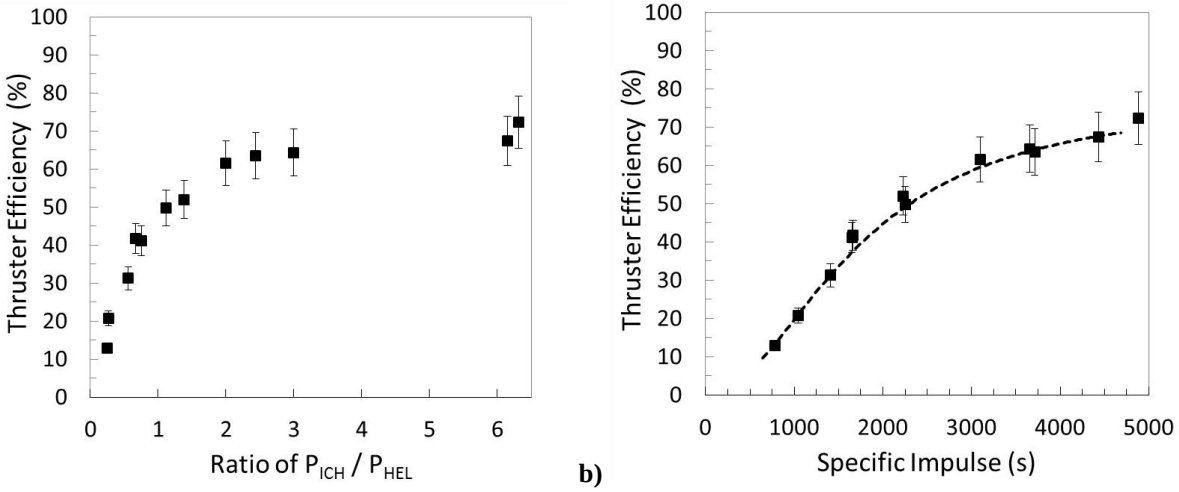

Figure 5. Thruster efficiency of the VX-200 engine as a function of the ICH RF Power to Helicon RF Power, a), and as a function of specific impulse, b). A least squares fit of the data to a semi-empirical model is also superimposed, dashed line.

Any change to the thruster efficiency was due largely to the increasing component of ICH coupled RF power. The limiting factor in the maximum ICH coupled RF power to the VX-200 engine was a vacuum pressure limit within the vacuum chamber, where greater RF circuit voltages produced glow or arc discharges that prompted the VX-200 engine solid state RF generators to shut down. The total thruster efficiency in Fig. 5 increases as a function of coupled ICH RF power and I_{sp}, indicating that the process of ICH wave coupling into the plasma column has not saturated.

Measurements of the ionization cost, defined as the ratio of the coupled RF power to the total ion current that is extracted from the system in the exhaust section, were taken during helicon-only operation as a function of both coupled RF power and argon propellant flow rate, from 15 kW to 35 kW and 50 mg/s to 160 mg/s respectively for argon and 100 to 250 mg/s for krypton. The lowest ionization cost measurement of 80±9 eV for argon and 70±9 eV for krypton occurred with VX-200 engine settings of 33 kW coupled RF power and 160 mg/s and 18 kW coupled RF power and 160 mg/s respectively. The ionization cost term, E_i, appears in Eqn 5. Though a small fraction of ICH power may be absorbed by electrons, for the purposes of the semi-empirical model in Eqn 5., it is assumed that the ICH process does not affect E_i.

A least squares fit to the data is used with a semi-empirical model of the thruster efficiency[11,23] for the VX-200 engine similar to Eqn. 5, where the ICH coupling efficiency is the only free parameter, such that

$$\eta_T = \frac{\frac{1}{2}m_{Ar}g^2I_{SP}^2}{eE_i + eE_1\left(1-\frac{1}{\eta_B}\right)+\frac{\frac{1}{2}m_{Ar}g^2I_{SP}^2}{\eta_B\eta_n}}, \quad \text{Eqn. 5}$$

where m_i is the atomic mass, g is the gravitational acceleration, I_{SP} is the specific impulse, e is the electron charge, E_i is the ionization cost of the propellant, E_1 is the first stage (helicon) RF power coupled to the plasma that is converted into directed ion kinetic energy through ambipolar acceleration, η_B is the ICH efficiency, and η_n is the nozzle efficiency. The ionization cost of the propellant for 29 kW helicon power and 107 mg/s Ar was E_i=105±9 eV/ion-extracted, the kinetic energy of ions leaving the first stage was E_1=22±2 eV, and the nozzle efficiency was η_n=97%. The only free parameter is the ICH coupling efficiency, η_B, which was fit to the data using a least squares algorithm, and was found to be 85%. It should be noted that η_B also includes the efficiency loss due to the ion energy spread in the exhaust, i.e. the frozen flow losses due to the finite ion temperature. Decreasing E_i or increasing E_1 shifts the semi-empirical model curve to the left and increasing η_B or η_N shifts the curve upward. The VX-200 engine helicon and ICH couplers were designed to produce a thruster efficiency of 60% at 5000 s using 200 kW DC input power (equivalent to 186 kW of coupled helicon and ICH RF power). The measured performance of the VX-200 using the full 200 kW of RF power revealed a 72% thruster efficiency at a specific impulse of 4900±300 s, significantly exceeding the performance and design specifications.

Doubly and Triply Ionized Species

No indication of secondary (Ar^{2+}) or tertiary (Ar^{3+}) ionization states were observed based on optical spectrometer measurements 0.3 m downstream of the VX-200 engine exit plane. This implies that the population of Ar^{2+} and Ar^{3+} ions is at least less than 1% of the Ar^{+} population. In addition, Ar^{2+} and Ar^{3+} ions are not detected to within 5% of the Ar^{+} population based on RPA data at a location of z = 0.4 m. This low fraction of Ar^{2+} and Ar^{3+} is somewhat unique to magnetoplasma thrusters as the acceleration mechanism is separated from the plasma generation mechanism. For the data presented in this paper, the ion-neutral charge exchange mean free path was 10 m.

B. Helicon Plasma Source Performance with Argon and Krypton

Experiments designed to measure the performance of the helicon plasma source stage were performed using krypton propellant over an applied RF power range from 10 to 33 kW and a propellant flow rate range from 100 to 250 mg/s. These experiments were reproduced with argon propellant for the same applied RF power range and a similar particle flow rate, though a different mass flow rate range of 50 to 160 mg/s. The efficiency of the helicon plasma source was characterized in terms of ionization cost of the propellant, Eqn 6, as well as the ionization fraction, Fig. 6. Unlike most thruster ionization cost characterizations, a conservative approach is taken and the ion current from the helicon plasma source is measured at the exit plane of the engine instead of *within* the core itself. This results in an effective ionization cost of *extracted* ions from the thruster. Precaution was also taken to ensure that the ion flux probes were biased $3T_e$ more negative than the plasma floating potential, ensuring that extra ion current was not collected as a result of ion impact ionization with the probe tip and excess electron reflection at the probe sheath.

$$E_i \equiv \frac{P_{helicon}}{\mathrm{I}_{ion}} - E_1 \quad \text{Eqn. 6}$$

The helicon performance data indicates that a larger operational envelope, in terms of RF power and propellant flow rate, is possible when using krypton propellant compared to argon propellant. This is somewhat expected since the ionization energy for krypton is lower than it is for argon, in addition to the fact that the thermal sound speed of neutral krypton atoms is slower than it is for argon which increases the neutral krypton residence time within the helicon source.

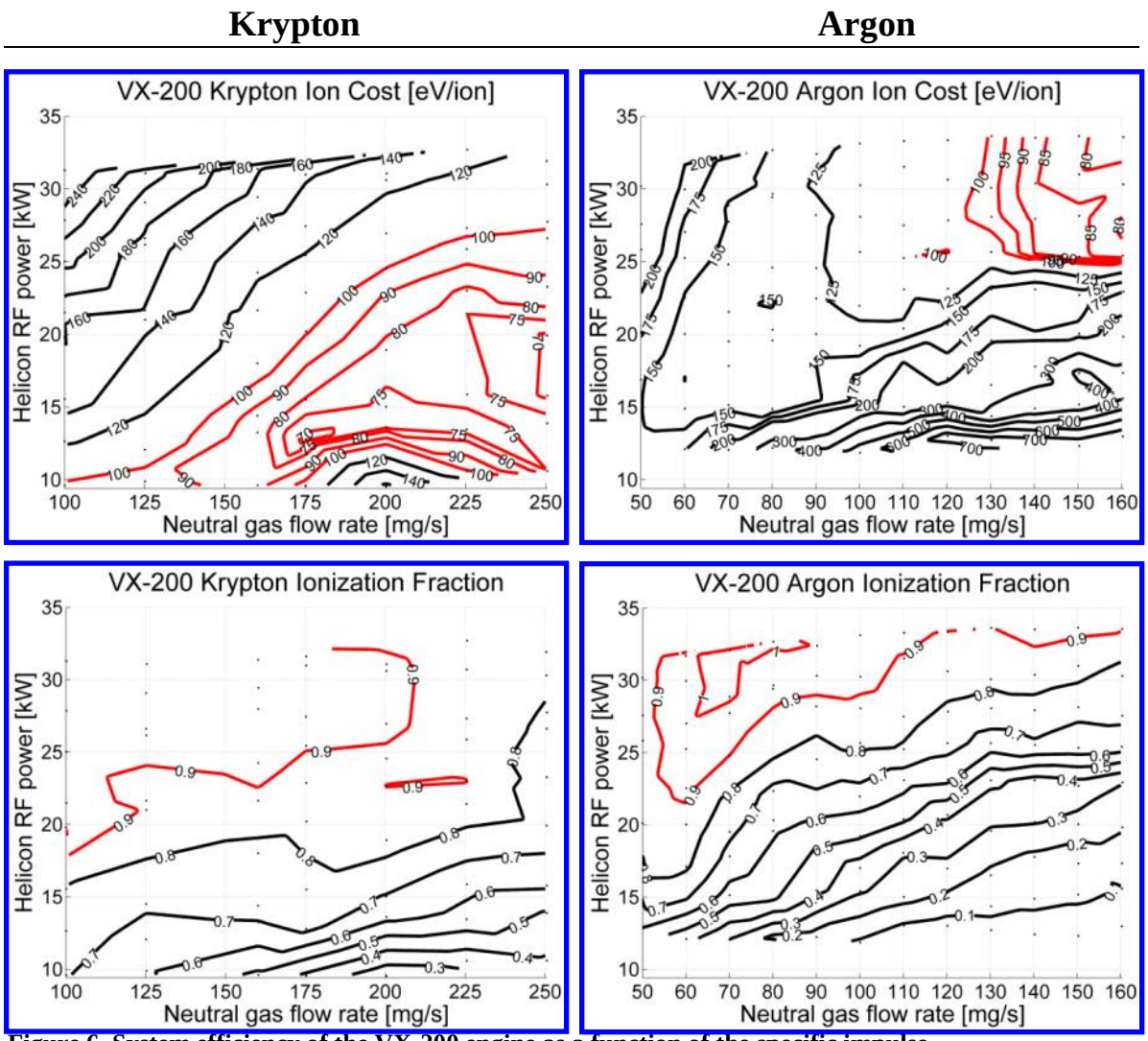

Figure 6. System efficiency of the VX-200 engine as a function of the specific impulse.

Metastable states play an important role in the ionization process of argon gas, which in some cases can act to decrease the effective ionization cost when compared to atoms that do not have many metastable states.[41,42] Not as much work has been performed with krypton metastables, though it is thought that this also plays an important role in the ionization process of krypton. The red lines on the ion cost graphs for krypton (left) and argon (right) in Fig. 6 show contour regions where the ion cost is less than 100 eV/ion, which is a desired design parameter of the plasma source for use within the VX-200. Note that the regions with ion cost below 100 eV/ion are much larger for krypton than with argon, indicating that for at least the current design of the VX-200, krypton is an attractive propellant option for near-term LEO applications. Regions as low as 70 eV/ion are possible with krypton propellant, and as low as 80 eV/ion with argon propellant within the helicon plasma source of the VX-200. Figure 6 also shows graphs of the ion fraction for both krypton propellant and argon propellant, where both regions of ion fraction greater than 90% are similar. It remains to be seen if krypton ICH will perform as well as argon ICH in terms of ICH efficiency and hence thruster efficiency. One complication is the multiple stable isotopes of krypton, which would tend to change the resonance location within the ICH stage. However, in simulations this location only changes by a distance on the order of millimeters.

The lower ionization cost for krypton, compared to argon, is positive for not only improving the helicon stage of the VX-200, but also being able to achieve higher T/P ratios during full ICH operations of the VX-200 prototype due solely to the increased thruster efficiency at lower specific impulse settings. This helicon performance work with krypton lays the groundwork for possible future performance measurements using full power ICH with the existing magnet of the VX-200 and an altered ICH generator frequency compared to the settings used for argon.

C. Semi-empirical Model of Krypton ICH Performance

One of the largest driving factors for electric propulsion thruster design is the cost of delivering payload to a desired destination. If the thruster designed for operations in and around Low Earth Orbit (LEO) out to Geostationary Earth Orbit (GEO), specific impulse values of ~1500 s to 4000 s are desired in order to reduce the cost of the power system (where solar panels are considered), and to shorten the trip time from higher taking advantage of higher T/P ratios at the expense of excessive specific impulse settings.

In order for the VX-200 to operate efficiently, defined here as a thruster efficiency exceeding 60% and a system efficiency exceeding 50%, a propellant with an atomic mass larger than 40 amu (Ar) must be used to produce >60% thruster efficiency at specific impulse values below 4000 s. For the VX-200, krypton propellant is attractive since it has a reduced ionization energy compared to argon and has an average atomic mass of 84 amu. Figure 7 shows modeled system efficiencies for the VX-200 operating with different propellant choices including krypton, argon, oxygen, nitrogen, and hydrogen for ion energies from 20 eV to 700 eV. Note that the hydrogen system efficiency does in fact exceed 60%, but at a specific impulse of ~30,000 s. Figure 7 also shows measured VX-200 system efficiency values (including superconducting magnet power supplies and laboratory cryocoolers) as a function of the measured specific impulse, up to a DC power level of 212 kW. The various propellant curves in Fig. 7 show ion energies from 20 eV up to 700 eV, which would go from a helicon-only operation of 30 kW (22 eV ambipolar ion acceleration) up to a system power level of 300 kW (30 kW Helicon RF Power, 270 kW ICH RF Power). An assumption is made that the helicon power level is fixed at 30 kW in Fig. 7.

For near-term applications in LEO, an Isp in the range of 1500 s to 2500 s is more desirable since, for a fixed power level, it reduces trip time. Krypton provides an interesting option for VX-200 operation in the LEO, MEO, and GEO environments due to the fact that a higher thruster efficiency is possible at a lower I_{sp}.

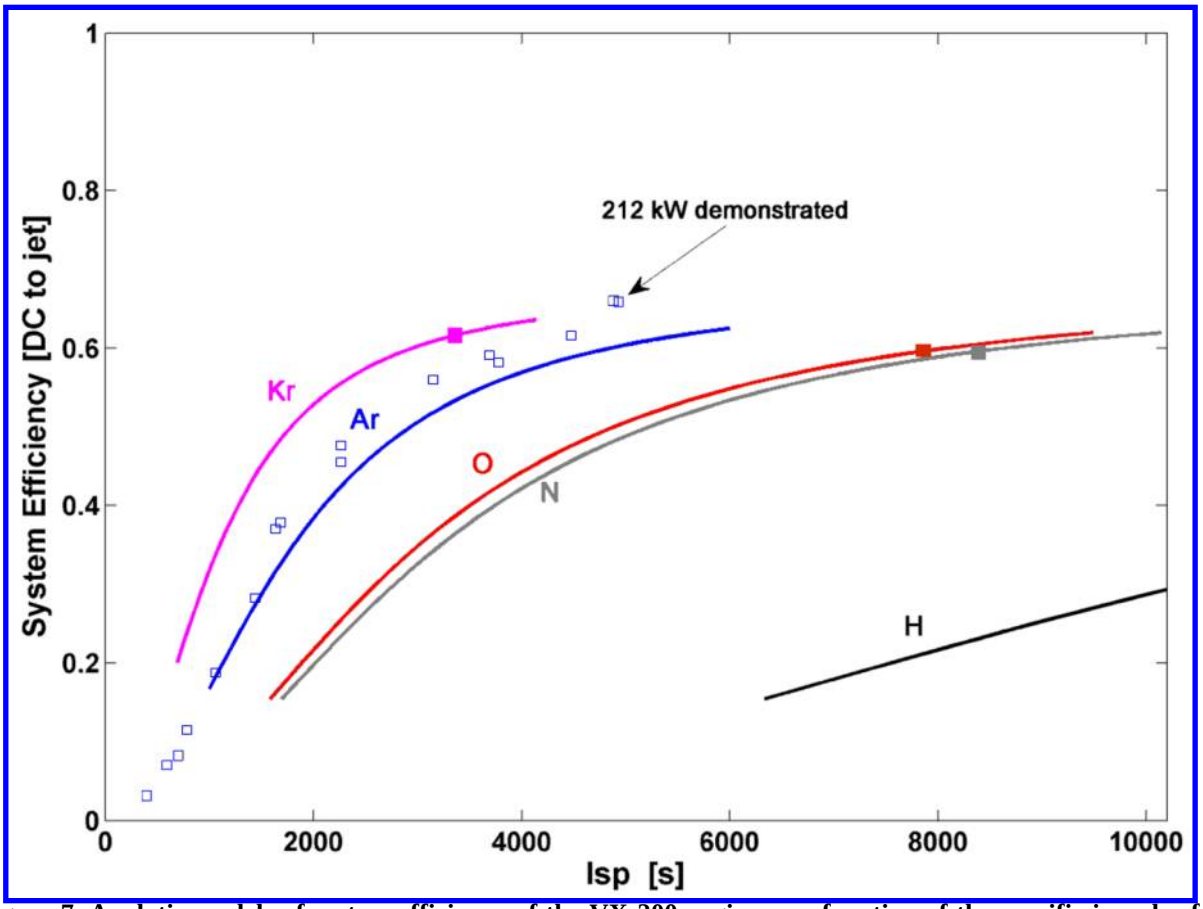

Figure 7. Analytic models of system efficiency of the VX-200 engine as a function of the specific impulse for various propellants (solid lines), and measured system efficiencies of the VX-200 lab prototype for argon (blue squares).

IV. Conclusion

The thruster efficiency and thrust of a high-power VASIMR prototype have been measured at a power level of 200 kW operating inside a vacuum chamber with sufficient volume and pumping to simulate the vacuum conditions of space. Using an ion flux probe array and a plasma momentum flux sensor (PMFS), the exhaust of the VX-200 engine was characterized as a function of the coupled RF power and as a function of the radial and axial position within the exhaust plume. A thruster efficiency of 72% was calculated using the force measurements and propellant flow rate with the specific impulse of 4880 s when operating at a total RF coupled power of 200 kW. The ionization cost of argon propellant was determined to be 80 eV/ion for optimized values of RF power and propellant flow rate for argon and 70 eV/ion for krypton. A semi-empirical fit to the full power performance data indicates an ICH coupling efficiency of 85% at 200 kW total RF power (212 kW total DC power). A high thrust-to-power operating mode was characterized over a wide parameter space with a maximum thrust to power ratio of 51 mN/kW at a specific impulse of 1660 s for a ratio of ICH RF power to Helicon RF power of 0.7:1. The extensive throttling optimization shows a thruster efficiency curve that exceeds 50% for a specific impulse of 2000 s and higher. This work paves the way for further development and operation with Krypton propellant, which should yield an improved thrust-to-power ratio and a higher thruster efficiency at a lower specific impulse, which is more closely optimized for spaceflight applications in Low Earth Orbit.

References

[1]Frisbee, R., "SP-100 Nuclear Electric Propulsion for Mars Cargo Missions," 29th AIAA/SAE/ASME/ASEE Joint Propulsion Conference, Monterey, CA, USA, June 1993, AIAA-93-2092.

[2]Frisbee, R., "Electric Propulsion Options for Mars Cargo Missions," 32nd AIAA/ASME/SAE/ASEE Joint Propulsion Conference and Exhibit, Lake Buena Vista, FL, USA, July 1996, AIAA-96-3173.

[3]Sankaran, K., Cassady, L., Kodys, A., and Choueiri, E., "A Survey of Propulsion Options for Cargo and Piloted Missions to Mars," Astrodynamics Space Missions and Chaos, edited by E. Belbruno, D. Folta, and P. Gurfil, Vol. 1017, Annals of the New York Academy of Sciences, New York, NY, USA, 2004, pp. 450-567.

[4]Ilin, A., Cassady, L., Glover, T., Carter, M., and Chang Díaz , F., "A Survey of Missions using VASIMR for Flexible Space Exploration," Tech. Rep. JSC-65825, NASA - JSC, April 2010.

[5]Boswell, R. W. and Chen, F. F., "Helicons: The early years, "IEEE Transactions of Plasma Science, Vol. 25, December 1997, pp. 1229-1244.

[6]Chen, F. F. and Boswell, R. W., "Helicons: The past decade, "IEEE Transactions of Plasma Science, Vol. 25, December 1997, pp. 1245-1257.

[7]Northrop, T.G., "The Adiabatic Motion of Charged Particles," American Journal of Physics, Volume 32, Issue 10, pp. 807-807 (1964).

[8]Roederer, J. G., "Dynamics of geomagnetically trapped radiation," Physics and Chemistry in Space, Berlin: Springer, 1970.

[9]Bering III, E.A., Chang Díaz,F.R., Squire,J.P., Glover, T.W., Carter, M.D., McCaskill, G.E., Longmier, B.W., Brukardt, M.S., Chancery, W.J., Jacobson, V.T., "Observations of single-pass ion cyclotron heating in a trans-sonic flowing plasma," Physics of Plasmas 17, 043509, 2010.

[10]Longmier, B., Bering, E., Carter, M., Cassady, L., Chancery, W., Chang Díaz, F., Glover, T., Hershkowitz, N., Ilin, A., McCaskill, G., Olsen, C., Squire, J., "Ambipolar Ion Acceleration in an Expanding Magnetic Nozzle," Plasma Sources Sci. Technol. 20 015007, 2011.

[11]Cassady, L.D., Longmier, B.W., Olsen, C.S., Ballenger, M.G., McCaskill, G.E., Ilin, A.V., Carter, M.D., Glover, T.W., Squire, J.P. , Chang Díaz, F.R., "VASIMR Performance Results," AIAA Paper 2010-6772, 46th AIAA/ASME/SAE/ASEE Joint Propulsion Conference & Exhibit, Nashville, TN, 25-28 July, 2010.

[12]Longmier, B.W., Bering, E.A., Squire, J.P., Glover, T.W., Chang Diaz, F.R., and Brukardt, M., "Exhaust Plume Measurements of the VASIMR VX-200," 50th Annual Meeting of the Division of Plasma Physics, Dallas, TX, 17-21 Nov., 2008.

[13]West, M. Charles, C., Boswell, R., Operating Radio Frequency Antennas Immersed in Vacuum: Implications for Ground-Testing Plasma Thrusters, J. Propulsion Power Vol. 26, No. 4, 2010.

[14]Olsen, C., Ion Flux Maps and Helicon Source Efficiency in the VASIMR VX-100 Experiment Using a Moving Langmuir Probe Array, Master's thesis, Rice University, February 2009.

[15]Longmier, B., Reid, B., Gallimore, A., Chang Díaz, F., Squire, J., Glover, T., Chavers, G., and Bering, E., "Validating a Plasma Momentum Flux Sensor to an Inverted Pendulum Thrust Stand," Journal of Propulsion and Power, Vol. 25, No. 3, May-June 2009.

[16]Chavers, G., and Chang-Díaz, F., Momentum flux measuring instrument for neutral and charged particle flows, Rev. Sci. Instrum. 73, 3500, 2002.

[17]Chavers, G., Chang-Diaz, F., Irvine, C., Squire, J., Momentum and heat flux measurements using an impact target in flowing plasma, J. Propulsion Power Vol. 22 PP. 637, 2006.

[18]Yanagi, R., and Kimura, I., New type of target for the measurement of impulse bits of Pulsed Plasma Thrusters, J. Spacecr. Rockets Vol. 19, no. 3, pp. 246-249, 1982.

[19]Grun, J., Ripin, B., Ballistic pendula for measuring the momentum of a laser- produced plasma. Review of Scientific Instruments, Vol. 53, No. 12, pp. 1878–1881, 1982

[20]Cohen, S., Zonca, F., Timberlake, J., Bennett, T., Cuthbertson, J., Langer,W., Motley, R., An instrument for measuring the momentum flux from atomic and charged particle jets. Review of Scientific Instruments, Vol. 61, No. 11, pp. 3586–3591, 1990.

[21]Takao, Y., Eriguchi, K., and Ono, K., A miniature electrothermal thruster using microwave-excited microplasmas: thrust measurement and its comparison with numerical analysis, J. Appl. Phys. 101 123307, 2007.

[22]Lunt, T., et al. Edge plasma pressure measurements using a mechanical force sensor on the tokamak ISTTOK. Plasma Physics and Controlled Fusion, Vol. 49, pp. 1783–1790, 2007

[23]Böhrk, H., Auweter-Kurtz, M., Thrust measurement of the hybrid electric thruster TIHTUS by a baffle plate J. Propulsion Power Vol. 25, No. 3, pp. 729-736, 2009.

[24]West, M., Charles, C., Boswell, R., A high sensitivity momentum flux measuring instrument for plasma thruster exhausts and diffusive plasmas, Review of Scientific Instruments, Vol 80, No. 053509, 2009.

[25]Makrinich, G., Fruchtman, A., Experimental study of a radial plasma source, Phys. Plasmas 16, 043507, 2009.

[26]Ling, J., West, M., Lafleur, T., Charles C., and Boswell, R., Thrust measurements in a low-magnetic field high-density mode in the helicon double layer thruster, J. Phys. D: Appl. Phys. 43 305203, 2010

[27]Chen, X., The impact force acting on a flat plate exposed normally to a rarefied plasma plume issuing from an annular or circular nozzle, J. Phys. D: Appl. Phys. 43 315205, 2010

[28]Whipple, E.C., "The ion trap-results in "Exploration of the upper atmosphere with the help of the third Soviet sputnik"," Proc. IRE 47, 2023, 1959.

[29]Parker, L.W., and Whipple, Theory of Spacecraft Sheath Structure, Potential, and Velocity Effects on Ion Measurements by Traps and Mass Spectrometers," E.C., J. Geophys. Res. 75, 4720, 1970.

[30]Minami, S., and Takeya, Y., J. "Ion temperature determination in the ionosphere by retarding potential analyzer aboard sounding rocket," J. Geophys. Res. 87, 713, 1982.

[31]Hutchinson, I.H., Principles of Plasma DiagnosticsCambridge University Press, Cambridge, 1987.

[32]Bering III, E.A., Chang Díaz, F.R., and Squire, J.P., "The uses of RF waves in space propulsion systems," Radio Sci. Bull. 310, 92, 2004.

[33]National Institute of Standards and Technology (NIST) atomic spectra database [online database] URL: http://physics.nist.gov/cgi-bin/AtData/lines_form [cited 26 January 2011]

[34]Cox, W., Charles, C., Boswell, R., and Hawkins, R., Spatial retarding field energy analyzer measurements downstream of a helicon double layer plasma, Appl. Phys. Lett., 93, 071505, 2008.

[35]Sutton, R., and Biblarz, O., Rocket Propulsion Elements, 7th edition, John Wiley & Sons, Inc., 2001.

[36]Ilin, A., Chang Díaz , F., Squire, J., Tarditi, A., Breizman, B., and Carter, M., "Simulations of Plasma Detachment in VASIMR," 40th AIAA Aerospace Sciences Meeting and Exhibit , Reno, NV, January 14-17 2002, AIAA 2002-0346.

[37]Arefiev, A. and Breizman, B., "Magnetohydrodynamic scenario of plasma detachment in a magnetic nozzle," Physics of Plasmas, Vol. 12, 2005.

[38]Jared P. Squire, Chris S. Olsen, Franklin R. Chang Díaz, Leonard D. Cassady, Benjamin W. Longmier, Maxwell G. Ballenger, Mark D. Carter, Tim W. Glover, Greg E. McCaskill, Edgar A. Bering, III, VASIMR VX-200 Operation at 200 kW and Plume Measurements: Future Plans and an ISS EP Test Platform, EPC-2011-154, 32nd International Electric Propulsion Conference, Wiesbaden Germany, September 11–15, 2011.

[39]Chris S. Olsen, Jared P. Squire, Benjamin W. Longmier, Maxwell G. Ballenger, Leonard D. Cassady, Mark D. Carter, Paul Cloutier, Andrew Ilin, Edgar Bering, Mathew Giambusso, Experimental determination of plasma detachment from the diverging magnetic nozzle of the VASIMR VX-200 Electric Thruster, 53rd Annual Meeting of the APS Division of Plasma Physics, Salt Lake City, Utah, November 14-18, 2011.

[40]R.R. Hofer, "High-Specific Impulse Operation of the BPT-4000 Hall Thruster for NASA Science Missions," 46th AIAA/ASME/SAE/ASEE Joint Propulsion Conference & Exhibit, Nashville, TN, AIAA 2010-6623, 25 - 28 July, 2010

[41]A.V. Phelps, J.P. Molnar, Lifetimes of Metastable States of Noble Gases, Phys. Rev. 89, 1202–1208 (1953)

[42]J.E. Velazco, J.H. Kolts, and D.W. Setser, Rate constants and quenching mechanisms for the metastable states of argon, krypton, and xenon, J. Chem. Phys. 69, 4357 (1978)